Chemistry–A European Journal
Research Article
doi.org/10.1002/chem.202403747
Chemistry Europe
European Chemical Societies Publishing
www.chemeurj.org

Hot Paper

Evolution Enhances Kemp Eliminase Activity by Optimizing Oxyanion Stabilization and Conformational Flexibility

Hiva Doustmohammadi,[a] Janet Sanchez,[a] Dhani Ram Mahato,[a] and Sílvia Osuna*[a, b]

Dedicated to Prof. Solà on his 60th birthday.

The base-promoted Kemp elimination reaction has been used as a model system for enzyme design. Among the multiple computationally designed and evolved Kemp eliminases generated along the years, the HG3-to-HG3.17 evolutionary trajectory is particularly interesting due to the high catalytic efficiency of HG3.17 and the debated role of glutamine 50 (Gln50) as potential oxyanion stabilizer. This study aims to elucidate the structural and dynamic changes along the evolutionary pathway from HG3 to HG3.17 that contribute to improved catalytic efficiency. In particular, we evaluate key variants along the HG3 evolutionary trajectory via molecular dynamics simulations coupled to non-covalent interactions and water analysis. Our computational study indicates that HG3.17 can adopt a catalytically competent conformation promoted by a water-mediated network of non-covalent interactions, in which aspartate 127 (Asp127) is properly positioned for proton abstraction and Gln50 and to some extent mutation cysteine 84 (Cys84) contribute to oxyanion stabilization. We find that HG3.17 exhibits a rather high flexibility of Gln50, which is regulated by the conformation adopted by the active site residue tryptophan 44 (Trp44). This interplay between Gln50 and Trp44 positioning induced by distal active site mutations affects the water-mediated network of non-covalent interactions, Gln50 preorganization, and water content of the active site pocket.

Introduction

Enzymes often exhibit high levels of efficiency, precision, specificity, and high catalytic activity, which are predominantly attributed to their well-preorganized active site pocket.[1] This preorganization results in a lower entropic penalty for the catalytic reaction within the protein environment as compared to the uncatalyzed reaction in water.[2] Enzymes also have the ability to adopt multiple conformations in solution,[3] a key feature for facilitating their adaptation towards new functions.[3,4] Proficient enzymatic catalysis therefore requires active site preorganization for efficiently stabilizing the transition state(s) along the reaction, and optimization of the conformational ensemble important for substrate binding and product release.[5]

Initial attempts to computationally design enzymes were focused on the base-promoted proton abstraction Kemp elimination reaction (Figure 1A). Kemp elimination was used as a model system for computational enzyme design,[6] as it is a simple and abiological reaction, although some examples of natural enzymes catalyzing this reaction have been reported.[7] The Kemp elimination follows a one-step mechanism in which 5-nitrobenzisoxazole (**1**) is deprotonated followed by the irreversible cleavage of the N–O bond to generate the negatively charged salicylonitrile product (**2**, Figure 1A). The reaction requires a base for deprotonation and an oxyanion hole to stabilize the developed negative charge with the breaking of the N–O bond.

The first Kemp eliminases computationally designed were created using the so-called *inside-out* protocol[6,8] centered on the *theozyme*[6,8] concept and the Rosetta match/design software,[9] although other approaches have been used along the years.[10] The low activity of the generated computational variants were then further engineered with directed evolution (DE), which introduced 10–15 mutations and led to much higher catalytic activities.[8,11] This yielded the highly active Kemp eliminase HG3.17, which provides a $6x10^8$ rate acceleration (in terms of k_{cat}/k_{uncat}) towards 5-nitrobenzisoxazole.[11d,e] HG3.17 was obtained from multiple rounds of DE starting from HG3, which is based on the computational design HG2 but contains an additional mutation (S265T) that enhances activity by limiting the active site flexibility. This substitution was predicted via molecular dynamics (MD) simulations focused on HG2.[11d] High resolution X-ray structures of HG3.17 (with two additional mutations to facilitate crystallization: E47N/N300D),[11e] as well as room-temperature X-rays in the absence and presence of the transition state analogue 6-nitrobenzisoxazole (TSA, 6NT) revealed a compact highly preorganized active

[a] H. Doustmohammadi, J. Sanchez, D. Ram Mahato, S. Osuna
Departament de Química, Institut de Química Computacional i Catàlisi, c/ Maria Aurèlia Capmany 69, Girona 17003, Spain
E-mail: silvia.osuna@udg.edu
[b] S. Osuna
ICREA, Pg. Lluís Companys 23, Barcelona 08010, Spain

Supporting information for this article is available on the WWW under https://doi.org/10.1002/chem.202403747

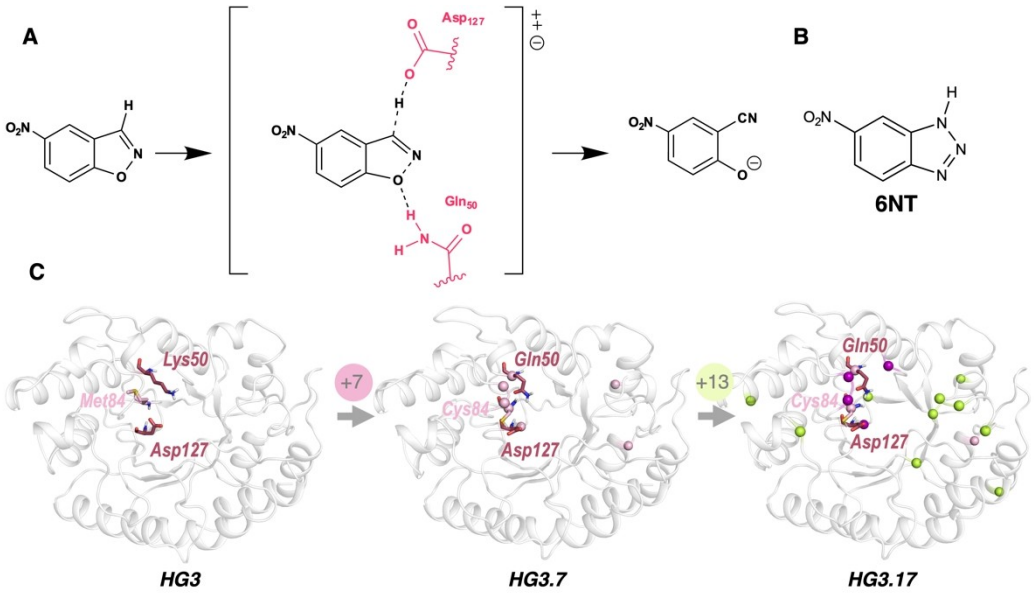

Figure 1. Representation of the (A) Kemp elimination reaction with 5-nitrobenzisoxazole as substrate, (B) the transition state analogue 6-nitrobenzisoxazole (TSA, 6NT), and (C) the HG3-to-HG3.17 evolutionary trajectory. The catalytic residues are shown as sticks and in raspberry, the mutations introduced are highlighted with colored spheres. Those positions mutated multiple times along the evolutionary trajectory are colored in violet.

site pocket with the catalytic base Asp127 properly positioned for catalysis.[12]

The 17 mutations introduced in HG3.17 were mostly located close to the active site pocket (11 out of 17), and three of them were mutated several times along the DE trajectory. Interestingly, out of the 17 DE mutations in HG3.17, two of them Lys50Gln and Met84Cys act synergistically and account for the major fraction of catalytic enhancement of HG3.17.[13] In light with this finding, high catalytic efficiencies were obtained if the core first and second-shell mutations of HG3.17 (the variant was named HG4) were considered.[12] By combining nuclear magnetic resonance, X-ray crystallography and stopped-flow kinetics, it was found that the DE mutations introduced in HG3.17 altered its conformational ensemble, thus promoting high-energy backbone reorganizations of strand 7 that positively preorganized the catalytic machinery for the proton transfer reaction.[13] Along the rounds of DE of particular interest is position 50, which was mutated from lysine to histidine, and afterwards from histidine to glutamine. HG3.7 is a DE intermediate variant that contains Gln50 as HG3.17. It was suggested that an additional reason for the enhanced activity of HG3.17 is the introduction of an oxyanion hole based on the new Gln50 residue introduced from HG.7 onwards, and an ordered water molecule.[11e] QM/MM simulations, however, indicated that water molecules could contribute to phenoxide stabilization and instead displace Gln50.[14] This observation is also in line with quantum mechanical (QM) calculations, which predicted water as the most effective general acid, reducing the uncatalyzed activation energy by ca. 9.5 kcal/mol.[15] Kinetic data and X-ray structures of several mutants replacing Gln50 into amino acids of different nature suggested that Gln50 as oxyanion hole contributes modestly to HG3.17 catalytic efficiency.[16] This observation is in line with previous studies evaluating the effect of the oxyanion contribution observed in proteases[17] and isomerases.[18] The effect of a single hydrogen bond to the anionic intermediate in ketosteroid isomerase was proposed to largely impact the catalytic activity (k_{cat}) of up to 10^5.[19] However, by replacing the oxyanion hole hydrogen donors with smaller residues allowing a higher water content in the active site cavity a small contribution of the oxyanion hole with respect to the solution reaction was observed.[18,19]

In a recent study, a hybrid computational strategy was developed to introduce additional mutations in HG3.17 to stabilize the catalytic conformation of Gln50, different mutants were generated that contained mutations around Gln50, which increased the catalytic efficiency of HG3.17 by up to 55 %.[20] These studies indicate that the role of Gln50 in the HG3.7–17 series is much more complex than originally thought. Of interest is that the starting HG3 enzyme[11d] and other Kemp eliminase designs[8,11a,21] lack an equivalent Gln at this position.

In this study, we aimed to computationally investigate by means of microsecond timescale molecular dynamics (MD) simulations three key variants along the evolutionary trajectory of the HG3 series, namely the starting HG3 scaffold, HG3.7 containing 7 mutations including Gln50 and Cys84, and the most evolved HG3.17. We assume the formation of an oxyanion along the reaction pathway and use a transition state analogue as a model of the transition state. We evaluate the influence of the conformation of the active site residue Trp44 on the flexibility and preorganization of Gln50, and evaluate how the hydrogen bonding and non-covalent network of interactions is altered along the evolutionary pathway. Our work provides some complementary analysis to elucidate the contribution of Gln50 and in a few conformations Cys84 as oxyanion stabilizer.

Results and Discussion

As mentioned in the introduction the high catalytic efficiency of HG3.17 has been evaluated by multiple experimental and computational techniques along the years,[11e,12–14,16,20–21] still the role of some of the suggested key mutations, namely Lys50Gln and Met84Cys, is not clear. We decided to computationally evaluate via multiple replica microsecond timescale MD simulations three key variants along the evolutionary pathway: the starting HG3 scaffold, the intermediate HG3.7 variant, and the most evolved HG3.17. We performed all atom MD simulations in the presence of the transition state analogue 6NT, which is the ligand present in all the liganded X-ray structures. However, we also considered the natural substrate benzoisoxazole (named 5NT) in the case of HG3 and HG3.17. As shown in a recent study, 6NT has a charge distribution closer to the TS especially at the deprotonation site,[22] thus making 6NT a suitable ligand for modeling the active site preorganization at the TS. To identify the key conformational changes taking place along the MD simulations of the three variants, we applied principal component analysis (PCA) considering all heavy atoms around 6 Å of 6NT (see SI for methods, Figure 2, 4, 6). As shown in Figures 2, 4 and 6, this analysis generates a conformational space in which each variant shares some minima with each other. Interestingly, we found that PC0 (x-axis) mostly involves distances between Trp87, and several residues contained in beta strands 1, 6–7 or loops L6, L7 and L18, whereas PC1 (y-axis) distances between Trp44, Met172, and Ile236 (see Figure S1).

HG3 Adopts a Trans Conformation of Beta Strand 3 and Lacks a Properly Preorganized Oxyanion Hole

The starting scaffold for the DE trajectory is HG3, which contains Lys50 and Met84 (instead of Gln50 and Cys84 as in the rest of the analyzed variants). The analysis of the available X-ray structures of HG3 with 6NT bound indicate that Gly83 and Met84 in the beta strand 3 can adopt both a cis and trans conformation (with occupancies of 0.6 and 0.3, respectively). This is observed both for unliganded and 6NT-bound structures (PDB: 5RG4, 5RGA, see Table S1 and Figure S1).[12] We therefore decided to perform MD simulations starting from the cis and trans conformations (PDB: 5RGA). The analysis of the conformational landscapes shown in Figure 2 indicates that HG3 can mostly adopt three main conformations in both cis and trans conformations. One additional interesting observation is that in all conformations sampled, the distance between 6NT and the catalytic Asp127 is well maintained, which is again in line with the TSA-bound structures obtained for HG3.[12] The analysis of the non-covalent interactions with NCIplot[23] at each conformation **1**–**3**, shows a blue strong attractive hydrogen bond between Asp127 and 6NT. In contrast, the analysis of the established interactions between 6NT and Lys50, suggested to play a role as oxyanion stabilizer in HG3, indicate a much weaker interaction (green interaction areas in NCIplot, Figure 2). Only in conformation **1** for both cis and trans and conformation **2** in cis, Lys50 adopts a better orientation for acting as oxyanion stabilizer and displays more favorable attractive (green blue) interaction. Interestingly, when the natural benzoisoxazole (named 5NT) substrate is used (instead of 6NT), much longer distances and substantially weaker interactions between 5NT and the catalytic Asp127 and Lys50 are observed, in line with a recent publication (Figure S3, S4).[22]

We observe in conformation **3** with the trans configuration of 83–84 peptide bond that the 6NT ligand is displaced from the active site pocket, and instead Trp44 positions its indole sidechain in the space left by 6NT. This reorganization of Trp44 perfectly matches one of the observed conformations of Trp44 in the unliganded X-ray structures (PDB: 5RG4, chain A), which also confirms the high flexibility of Trp44.[12] In this new conformation, the nitrogen of the indole sidechain of Trp44 establishes a hydrogen bond with the catalytic aspartate Asp127. The latter is hydrogen bonded at the same time to 6NT, despite the fact TSA being displaced from the active site pocket (see Figure 2B, conformation **3**). Instead, the interaction with Lys50 is lost in this conformation **3** (distance between 6NT and Lys50 of ca. 14 Å, see Figure 2B conformation **3**). This new conformation of 6NT is stabilized by the non-covalent interactions established with Arg124, Tyr17, Trp44, Met42, Tyr170, as shown by the NCIplot analyses (see Figure 2). This conformation **3** in which 6NT is displaced from the active site observed when the 83–84 peptide bond is in a trans conformation is not sampled in the case of cis.

It should be also mentioned that Met84 is highly flexible in HG3. This position is mutated into a cysteine in both HG3.7 and HG3.17. The analysis of the water content of the active site by means of GIST analysis,[24] indicates that the conformation adopted by Met84 has an effect into the water network and entrance into the pocket (Figure 3). The water content in both cis and trans conformations is rather low.

HG3.7 Adopts a Cis Conformation of Beta Strand 3 and a Proper Preorganization of Gln50 as Oxyanion Stabilizer

The introduction of 7 mutations in HG3 generates the intermediate HG3.7 variant, which contains the same catalytic machinery (Asp127 and Gln50) as HG3.17. This intermediate variant also contains Met84Cys mutation, which was found to act synergistically with Lys50Gln.[13] Interestingly, the introduced mutations favor the stabilization of the cis conformation of the Gly83 and Cys84 peptide bond, as shown by 6NT-bound X-ray structures (PDB: 5RGC,[12] and 7 K4X,[13] see Table S1).

In all **1**–**3** conformations sampled, the catalytic Asp127 and the new Gln50 are positioned close to 6NT (see Figure 4). NCI analysis indicates a strong attractive interaction between Asp127 and 6NT in all sampled conformations, however, the Gln50–6NT interaction is much weaker (green region instead of blue in all minima, Figure 4). Still, the flexibility of Gln50 is substantially reduced as compared to the equivalent Lys50 in HG3, thus indicating a much better preorganized active site pocket in HG3.7 for the proton transfer reaction. The rigidity of Gln50 is mostly attributed to the hydrogen bond established

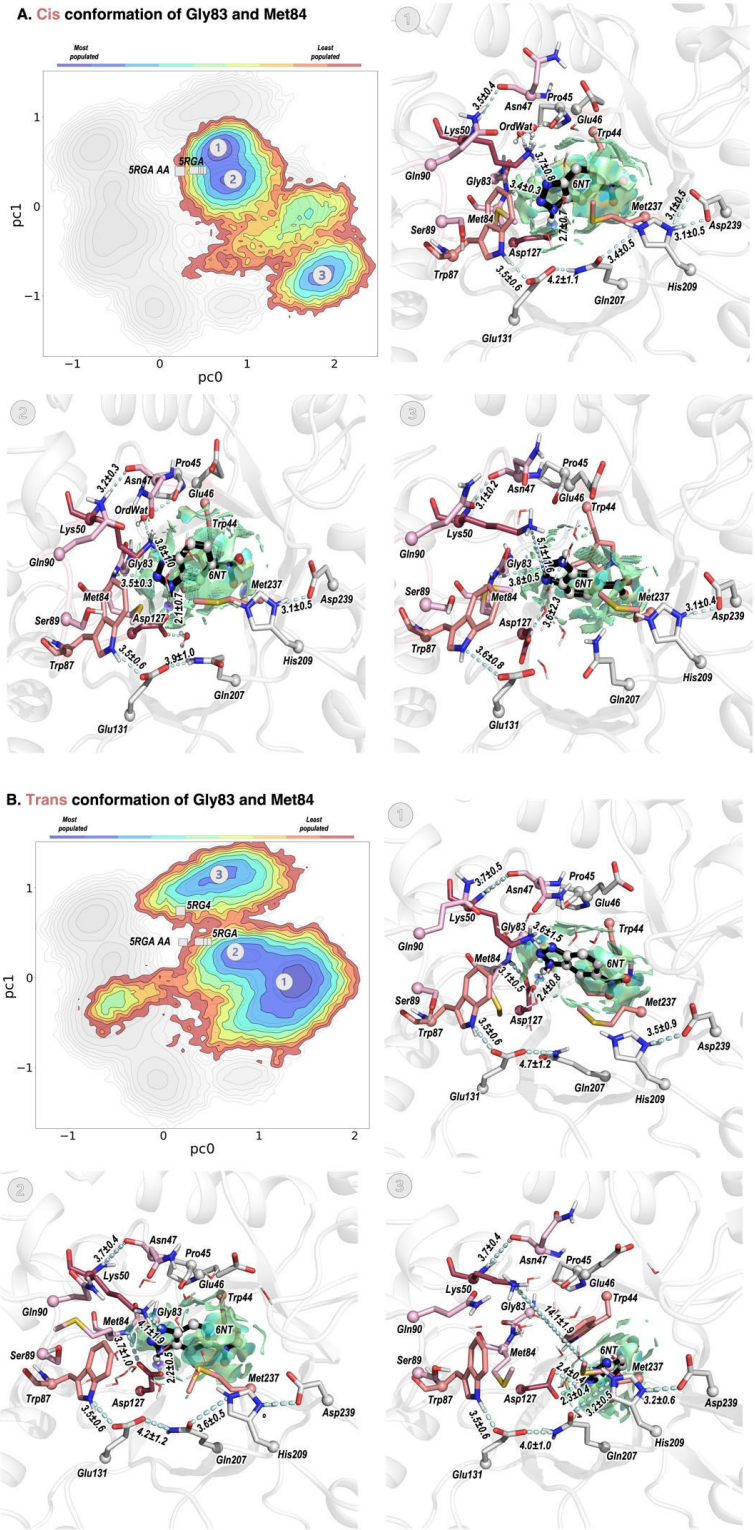

Figure 2. Reconstructed conformational landscapes of HG3 in the presence of 6NT considering: (**A**) the cis conformation of Gly83 and Met84 (conformation with the highest occupation in X-ray 5RGA), and (**B**) the trans conformation. Conformational landscape reconstruction is based on the combined HG3-to-HG3.17 PCA analysis: PC0 (x-axis) mostly involves distances between Trp87, and several residues contained in beta strands 1, 6–7 or loops L6, L7 and L18, whereas PC1 (y-axis) distances between Trp44, Met172, and Ile236 A representative structure of each sampled conformation is shown. The non-covalent interactions (as described by NCI analysis[23]) established between 6NT and the active site pocket are shown: the strong attractive interactions are displayed with a blue mesh, weak non-covalent interactions in green, and repulsive interaction in red. The mean distance together with standard deviation for the catalytically relevant distances involving 6NT and Asp127, and Lys50 are shown for each minimum. Catalytic and binding residues are shown in sticks and colored in raspberry, whereas the mutations in light pink. 6NT is shown as spheres and black sticks. The most important interactions are also highlighted with a dashed cyan discontinuous line. Available crystallographic structures are projected on the same PC space. Those X-ray structures containing more than one chain, and different cis/trans conformations are all individually projected (marked with gray boxes).

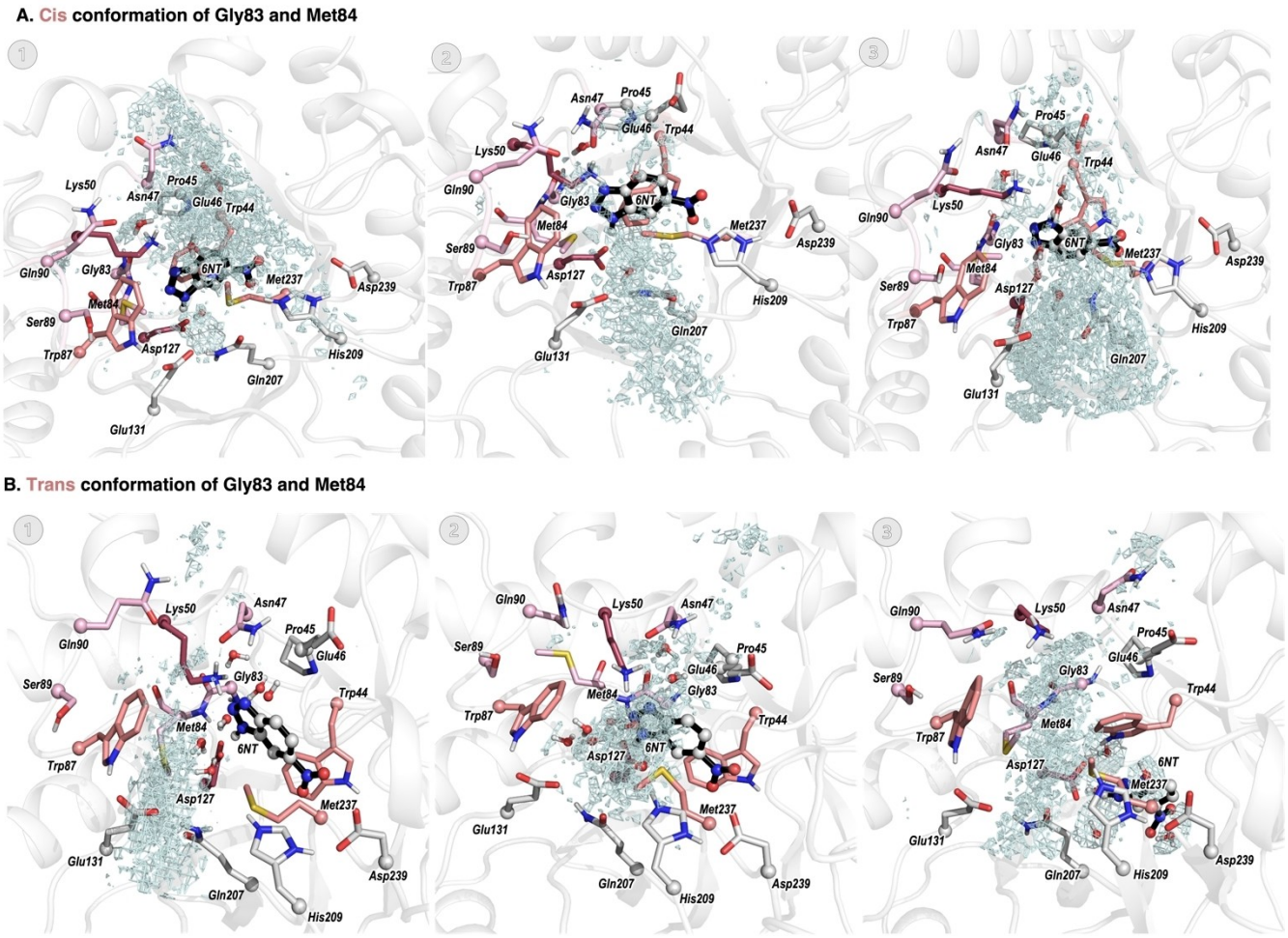

Figure 3. Analysis of the water content of the active site of HG3 in the presence of 6NT by means of GIST analysis[24] is shown using a blue mesh on a representative structure of each minima in the conformational landscape as shown in Figure 2A–B. Catalytic and binding residues are shown in sticks and colored in raspberry, whereas the mutations in light pink. 6NT is shown as spheres and black sticks.

between the carbonyl group of the sidechain and the amide backbone of Cys84.

Interestingly, there is a water molecule that contributes to this rigidification by establishing a hydrogen bond with the carbonyl backbone of Cys84 and sidechain of Gln50. The thiol group of the new Cys84 introduced establishes a hydrogen bond with the other oxygen of the carboxyl group of the catalytic Asp127, which favors Asp127 preorganization for catalysis. This is observed mostly in conformation **2** (and later in HG3.17, see below), however, in conformation **3** Cys84 is hydrogen bonded to the same oxygen of the carboxylate of Asp127 in charge of proton abstraction. Such interaction affects the nucleophilicity of Asp127 as demonstrated by the substantially weaker interaction (green area in NCI analysis) between 6NT and Asp127 (see Figure 4). Although Trp44 adopts only one major conformation in the 6NT-bound X-ray structure 7K4X,[13] two different conformations are observed in the 6NT-bound room temperature X-ray structure (PDB: 5RGC[12]), being the rotamer with the indole nitrogen pointing outside the active site pocket the one with the highest occupancy (which is the same one obtained in 7K4X).[13] Our simulations starting from the highest occupancy rotamer show that Trp44 is rather stable in this pose, and together with Met237 establish π-π and CH-π interactions with 6NT, respectively, as shown with the NCI analysis.

Another interesting observation is that the water content of the active site of HG3.7 is rather low: mostly one ordered water molecule is found and establishes a hydrogen bond with the carbonyl group of Gly83 potentially stabilizing the cis conformation of Gly83-Cys84 peptide bond. There is another water molecule hydrogen bonded to Gln50, and two of the residues mutated twice along directed evolution, *i.e.*, Ser89Arg, and Gln90His, also establish hydrogen bond interactions with the few water molecules found in the active site. Interestingly, in conformation labeled as **3**, Arg89 is displaced from the active site, which enhances the water accessibility to the pocket, as shown by the GIST[24] analysis (see Figure 5). Arg89 is mutated to Asn in HG3.17.

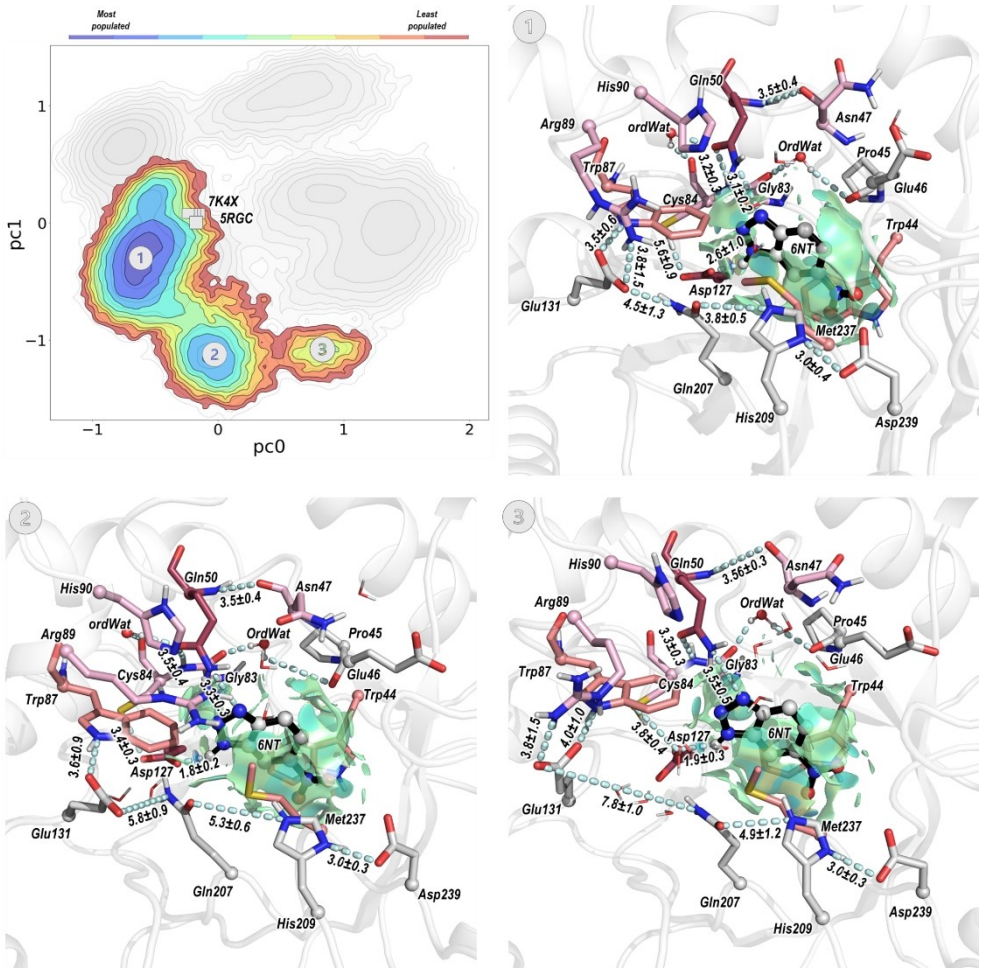

Figure 4. Reconstructed conformational landscape of HG3.7 in the presence of 6NT based on the combined HG3-to-HG3.17 PCA analysis: PC0 (x-axis) mostly involves distances between Trp87, and several residues contained in beta strands 1, 6–7 or loops L6, L7 and L18, whereas PC1 (y-axis) distances between Trp44, Met172, and Ile236. A representative structure of each sampled conformation is shown. The non-covalent interactions (as described by NCI analysis[23]) established between 6NT and the active site pocket are shown: the strong attractive interactions are displayed with a blue mesh, weak non-covalent interactions in green, and repulsive interaction in red. The mean distance together with standard deviation for the catalytically relevant distances involving 6NT and Asp127, and Gln50 are shown for each minimum. Catalytic and binding residues are shown in sticks and colored in raspberry, whereas the mutations in light pink. 6NT is shown as spheres and black sticks. The most important interactions are also highlighted with a dashed cyan discontinuous line. Available crystallographic structures are projected on the same PC space. Those X-ray structures containing more than one chain are all individually projected (marked with gray boxes).

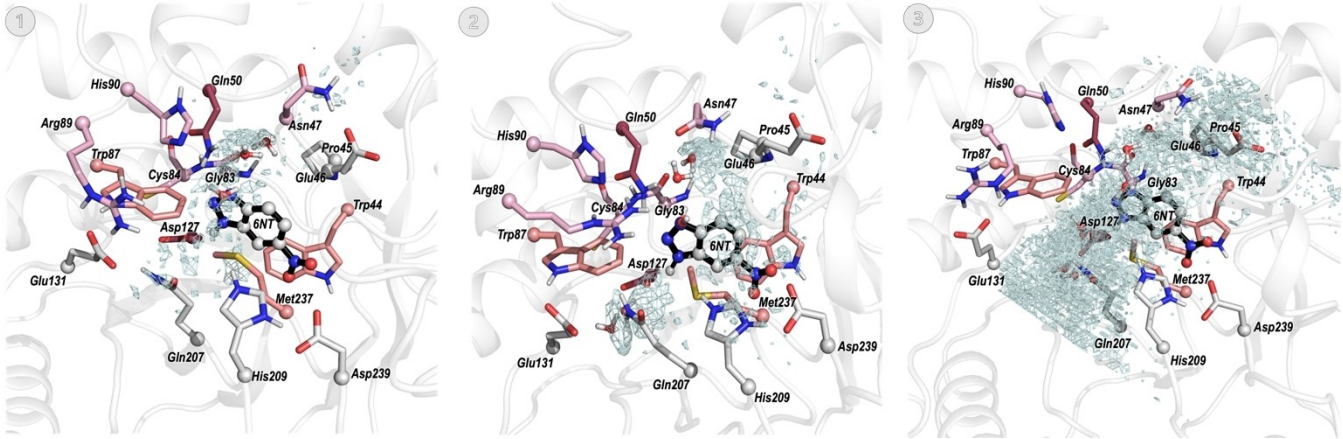

Figure 5. Analysis of the water content of the active site of HG3.7 in the presence of 6NT by means of GIST analysis[24] is shown using a blue mesh on a representative structure of each minima from the conformational landscape shown in Figure 4. Catalytic and binding residues are shown in sticks and colored in raspberry, whereas the mutations in light pink. 6NT is shown as spheres and black sticks.

HG3.17 Catalytic Activity is Enhanced Thanks to Increased Active Site Water Content and Gln50 Flexibility Regulated by Trp44 and Trp80 Conformation

The introduction of 13 mutations in HG3.7 resulted in HG3.17, which enhanced the Kemp eliminase reaction by 1.5-fold with respect to HG3.7 in terms of k_{cat}.[13] The minima obtained from the reconstructed conformational landscape shows that similarly to what is found for HG3 and HG3.7, the cis conformation of the Gly83-Cys84 peptide bond is stable (in line with X-ray data, see Table S1). This cis conformation is stabilized by the presence of an ordered water molecule that is hydrogen bonded to the carbonyl backbone of Gly83 and Pro45 (Figure 6A). The ordered water molecule also establishes a hydrogen bond with the sidechain of Gln50 in conformation **2 A**. Gly83 is additionally establishing a hydrogen bond with the indole nitrogen of Trp44, which has a different sidechain conformation compared to HG3.7 and allows the establishment of this new interaction. This water-mediated hydrogen bond network helps positioning the amide backbone of Cys84 backbone close to the nitrogen atom of 6NT corresponding to the position in which the developing negative charge on the phenoxide leaving group of the substrate will be located. The characterization of such interaction by means of NCI analysis indicates that a strong attractive interaction is found between the nitrogen atom of 6NT and the amide of Cys84, especially in conformation **2 A**, thus suggesting the backbone of Cys84 can also play a role as oxyanion stabilizer (Figure 6A). This contrasts with what was found in HG3.7, as the backbone of Cys84 is instead interacting with the sidechain of Gln50. Similarly to what is observed in HG3.7, in conformation **2 A** and **3 A** the thiol group of Cys84 establishes a hydrogen bond with one of the oxygen atoms of the catalytic Asp127, which is well positioned for proton abstraction in all sampled **1**–**3 A** conformations. This hydrogen bond interaction between Cys84 and the catalytic Asp127 was also found by Świderek et al. in the QM/MM studies of monomer B of the 4BS0 X-ray structure.[14] Interestingly, in this conformation **2 A** the carbonyl group of the amide of Gln50 is hydrogen bonded to the indole of Trp87, which helps positioning Gln50 close to 6NT. Of note is that such interaction between Gln50 and Trp87 is possible due to the flipped conformation of Trp87 as compared to HG3.7 and HG3. In fact, in HG3 and HG3.7 the indole nitrogen of Trp87 is hydrogen bonded to Glu131. A key mutation to maintain Trp87 in this flipped orientation is Arg89Asn. This position mutated twice along evolution introduces an amide for establishing the hydrogen bond with Glu131. Trp44 can also display two different possible rotamers according to the available 6NT-bound X-ray structures (PDB: 5RGE,[12] 4BS0,[11e] Table S1): in rotamer A Trp44 positions the indole nitrogen towards the catalytic Asp127 (rotamer A has a higher occupancy in X-ray), or it adopts the same rotamer as in HG3.7 in which the nitrogen of the indole ring does not point toward the active site (rotamer B, lower occupancy in X-ray data). As found previously in Świderek et al. study, we observe that Gln50 is extremely flexible in HG3.17 when rotamer A of Trp44 is considered (Figure 6),[14] and only in conformation **2 A** it is properly positioned for potentially contributing to stabilize the oxyanion. In the other conformations sampled (**1 A** and **3 A**), Gln50 is displaced from the active site, thus providing additional space, and allowing the entering of multiple water molecules in the pocket (Figure 7A). This flexibility of Gln50 is accompanied by conformational changes of Glu46 and Glu47, that again are important for enhancing the water content of the active site pocket. Glu47 corresponds to one of the introduced mutations, in HG3.7 it is an Asn47 instead. In conformation **2 A**, the carbonyl backbone of Glu47 is hydrogen bonded to the amide backbone of the catalytically relevant Gln50. The sidechain of Gln50 establishes a hydrogen bond with the nitrogen of the indole of Trp87, and with the ordered water molecule as explained above. A network of hydrogen bonds is observed within the water molecules contained in the active site pocket. Such network also includes the sidechain of Gln207 that at the same time makes a hydrogen bond with Glu131. Glu131 can interact with the sidechain of two introduced mutations in HG3.17, i.e., Arg89Asn and His90Phe. Both positions are mutated twice along the HG3-to-HG3.17 evolution.

Although rotamer B of Trp44 has a lower occupancy in the 6NT-bound X-ray structures (both in 4BS0[11e] and 5RGE[12]), additional MD simulations starting from this other conformation of Trp44 were performed (Figure 6B). Interestingly, Gln50 is substantially more rigid with this different conformation of Trp44, as the distance between its sidechain and 6NT is ca. 3 Å in all sampled **1 B**-**3 B** conformations (Figure 6B). The proper positioning of Gln50 for oxyanion stabilization is favored thanks to its interaction with the nitrogen of the indole of Trp87, and an ordered water molecule that links via hydrogen bonding Gln50 and the backbone of Pro45. As observed before, the catalytic Asp127 is properly positioned in all conformations. In conformation **3 B**, Cys84 is hydrogen bonded with one of the carboxyl oxygens of Asp127, as observed in **3 A**. The water content of the active site considering this additional rotamer of Trp44 is also high (Figure 7B).

Altogether this analysis suggests that HG3.17 enhanced Kemp eliminase activity is attributed to the fine-tuned network of water-mediated hydrogen bond interactions taking place along the catalytic pocket, which precisely position the catalytic and binding residues for catalysis. This precision in attaining the catalytically competent pose is mostly affecting the oxyanion hole residues, composed the debated Gln50 sidechain.[16] As shown with the NCI analysis in conformation **2 A** both Gln50 and Cys84 can additionally act as oxyanion hole and display strong attractive interactions with 6NT. This finding is in line with the synergistic effect observed experimentally by Cys84 and Gln50 in HG3.17.[13]

Our simulations also indicate that this precision observed in conformation **2 A** is complemented by a rather high flexibility of Gln50. Interestingly, Gln50 flexibility depends on Trp44 conformation: when the indole nitrogen of Trp44 points towards the catalytic residues, Gln50 is easily displaced from the active site (Figure 7A). However, the positioning of Trp44 in rotamer B helps maintaining Gln50 close to 6NT through the establishment of a hydrogen bond with Pro45 backbone via an ordered water molecule and with the indole nitrogen of Trp87. This hydrogen bond with Trp87 is possible thanks to the new positioning of the indole sidechain in HG3.17 (in HG3, and HG3.7 Trp87 instead interacts with Glu131). Such flexibility of Gln50 regulated by Trp44 conformation might potentially help the substrate binding/

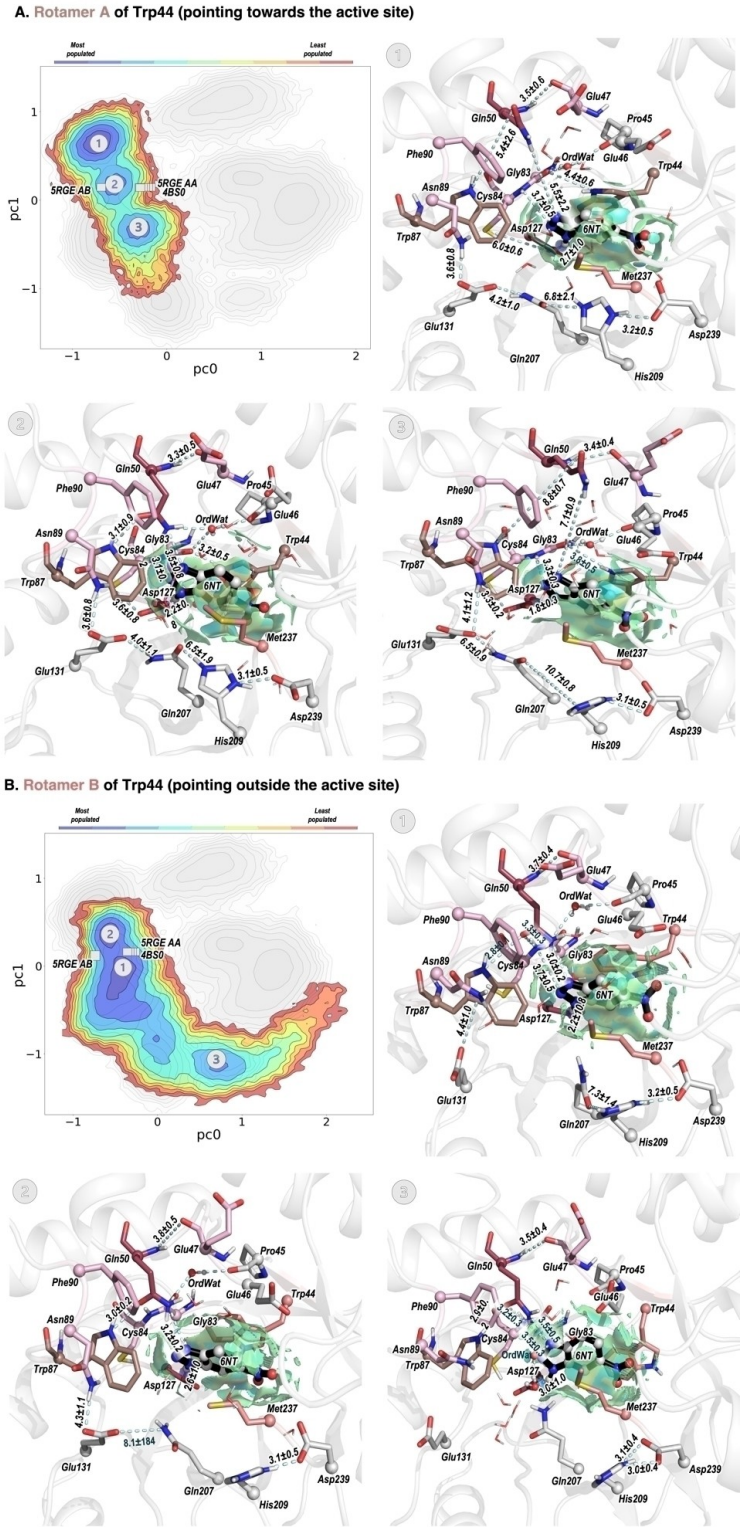

Figure 6. Reconstructed conformational landscape of HG3.17 in the presence of 6NT considering either (**A**) rotamer A of Trp44 presenting the nitrogen of the indole ring pointing towards Gly83, or (**B**) rotamer B of Trp44 with the indole nitrogen pointing out of the active site pocket. PC0 (x-axis) mostly involves distances between Trp87, and several residues contained in beta strands 1, 6–7 or loops L6, L7 and L18, whereas PC1 (y-axis) distances between Trp44, Met172, and Ile236. A representative structure of each sampled conformation is shown. The non-covalent interactions (as described by NCI analysis[23]) established between 6NT and the active site pocket are shown: the strong attractive interactions are displayed with a blue mesh, weak non-covalent interactions in green, and repulsive interaction in red. The mean distance together with standard deviation for the catalytically relevant distances involving 6NT and Asp127, and Gln50 are shown for each minimum. Catalytic residues are shown in sticks and colored in raspberry, whereas the mutations in light pink. 6NT is shown as spheres and black sticks. The most important interactions are also highlighted with a dashed cyan discontinuous line. Available crystallographic structures are projected on the same PC space. Those X-ray structures containing more than one chain and two rotamers of Trp44 are all individually projected (marked with a gray box). Rotamer A presenting the indole nitrogen pointing towards the catalytic Asp127 is the one with the highest occupation in the reported X-ray structures 5RGE and 5RG8 (occupation of 0.6/0.4 for rotamer A/B).

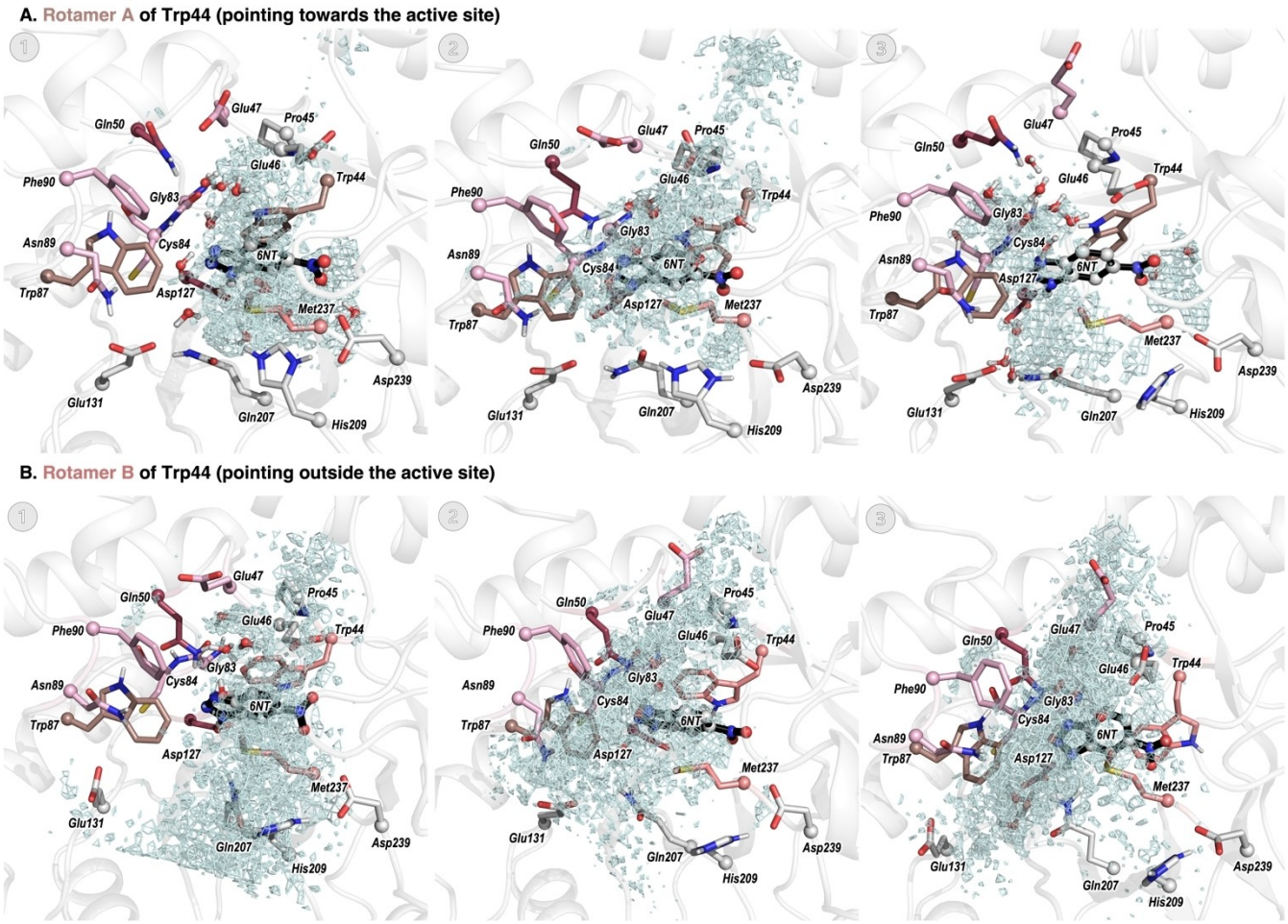

Figure 7. Analysis of the water content of the active site by means of GIST analysis[24] is shown using a blue mesh on a representative structure of each minima in the conformational landscape shown in Figure 6A–B. Catalytic and binding residues are shown in sticks and colored in raspberry, whereas the mutations in light pink. 6NT is shown as spheres and black sticks.

product release process, which is also in line with the experimental finding of an induced-fit process observed only in HG3.17.[13] Interestingly, in the X-ray structure of HG4 variant reported by Chica and coworkers, [12] which only contains HG3.17 active site mutations, the two possible rotamers of Trp44 are also observed. However, the rotamer with the highest occupancy corresponds to the conformation in which the indole nitrogen of Trp44 points away from the catalytic pocket (as it happens in HG3.7). Another interesting point is the conformation of Trp87, which points towards Glu131 as in HG3-HG3.7, therefore a direct hydrogen bond with Gln50 as observed in HG3.17 is not possible. This suggests that the distal mutations introduced along DE alter the positioning of Trp87 and Trp44, which according to our simulations influence Gln50 preorganization and the water content of the active site.

The evaluation of HG3.17 considering the natural benzoisoxazole (labeled 5NT) substrate provides similar insights to those obtained with 6NT. When Trp44 is positioned towards the active site short distances between the catalytic Asp127 and the deprotonation site of 5NT are observed, as well as a high flexibility of Gln50 is revealed (Figure 8A). However, as opposed to 6NT a longer distance and thus a weaker non-covalent interaction between the amide backbone of Cys84 and the nitrogen atom of 5NT is observed (Figure 8A). When the other rotamer of Trp44 is considered, the binding of the 5NT substrate is stable and establishes short distances with both catalytic Asp127 and Gln50, as observed with 6NT (Figure 8B).

Conclusions

The evaluation of the conformational dynamics of three Kemp eliminase variants within the HG3-to-HG3.17 evolutionary progression has revealed important differences in the flexibility, network of interactions and water content within the active site pockets. These variants include the initial HG3 scaffold, HG3.7 that incorporates 7 mutations including the synergistic Gln50 and Cys84, and the most evolved variant, HG3.17. Our analysis focuses on assessing the modifications in flexibility, hydrogen bonding, water content, and non-covalent interaction networks throughout this evolutionary pathway. Our results indicate that in HG3 both the trans and cis conformations of the peptide bond of Gly83 and

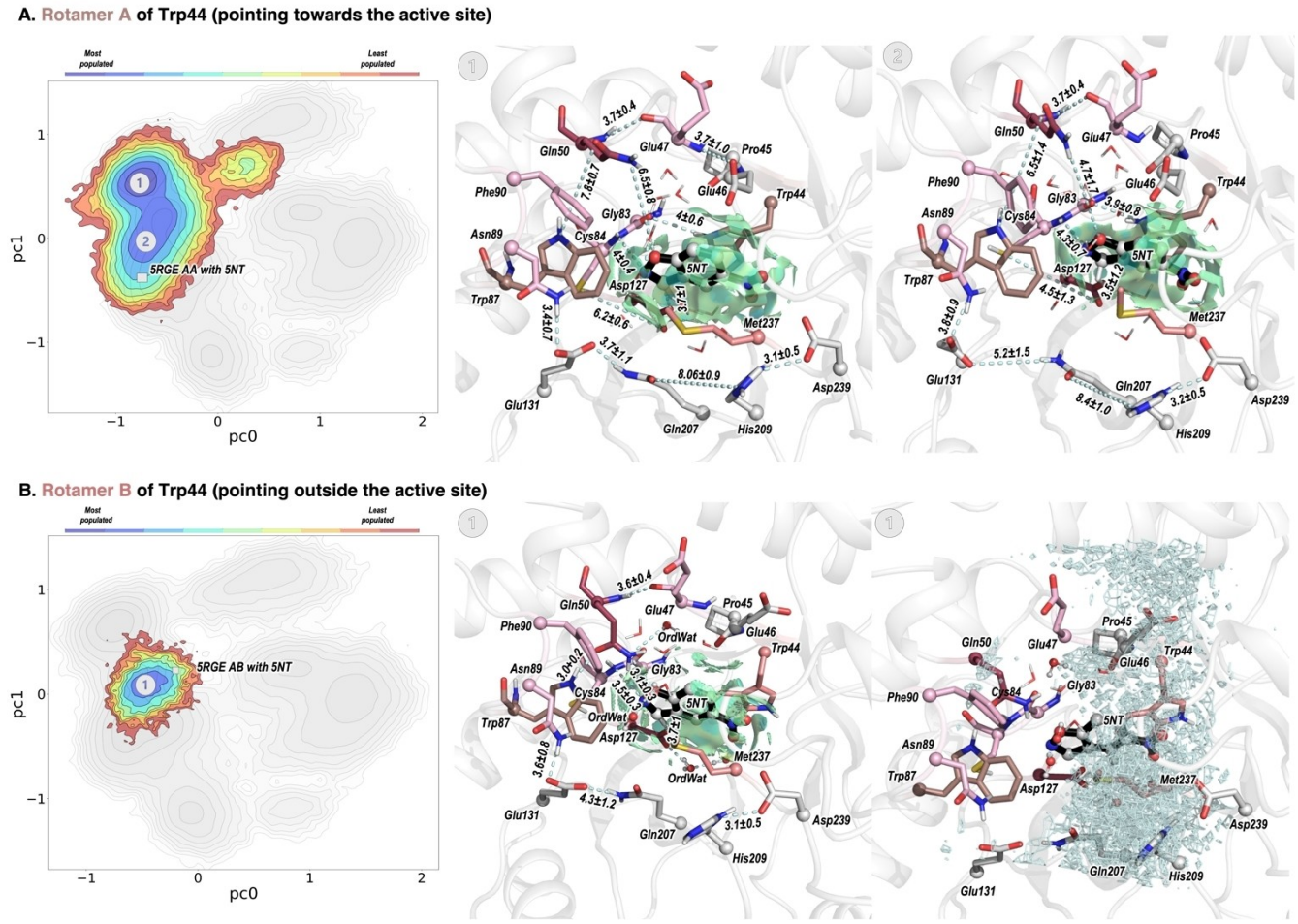

Figure 8. Reconstructed conformational landscape of HG3.17 in the presence of the substrate 5NT considering either (**A**) rotamer A of Trp44 presenting the nitrogen of the indole ring pointing towards Gly83, or (**B**) rotamer B of Trp44 with the indole nitrogen pointing out of the active site pocket. PC0 (x-axis) mostly involves distances between Trp87, and several residues contained in beta strands 1, 6–7 or loops L6, L7 and L18, whereas PC1 (y-axis) distances between Trp44, Met172, and Ile236. A representative structure of each sampled conformation is shown. The non-covalent interactions (as described by NCI analysis[23]) established between 6NT and the active site pocket are shown: the strong attractive interactions are displayed with a blue mesh, weak non-covalent interactions in green, and repulsive interaction in red. The mean distance together with standard deviation for the catalytically relevant distances involving 5NT and Asp127, and Gln50 are shown for each minimum. Catalytic residues are shown in sticks and colored in raspberry, whereas the mutations in light pink. 5NT is shown as spheres and black sticks. The most important interactions are also highlighted with a dashed cyan discontinuous line. For conformation 1B, the analysis of the water content of the active site by means of GIST analysis[24] is shown using a blue mesh. Those X-ray structures are projected (marked with a gray box).

Met84 contained in the beta strand 3 are stable under the studied MD simulation time. Even though the catalytic Asp127 is properly positioned for catalysis and establishes strong attractive interactions with 6NT, HG3 lacks a properly preorganized oxyanion hole (Lys50) for stabilizing the developed negative charge along the Kemp eliminase reaction. This is observed with both the transition state analogue 6NT and the natural substrate 5NT. This is substantially improved in HG3.7 that contains the key mutations Gln50 and Cys84. These mutations favor the cis conformation of the peptide bond of Gly83 and Cys84 (Met84 in HG3), which helps positioning Gln50 in place for acting as oxyanion stabilizer. In HG3 and HG3.7 variants, both Trp44 and Trp87 position the indole nitrogen pointing outside the active site pocket. A very low water content is observed in the active site of HG3.7, which contrasts with the most active HG3.17. Interestingly, we find that in one of the sampled conformations of HG3.17 both Gln50 and Cys84 can directly act as oxyanion stabilizers. Both residues either via sidechain (Gln50) or backbone (Cys84) establish strong attractive hydrogen-bond interactions with 6NT. Gln50 displays a high flexibility, especially when the active site Trp44 residue positions the indole nitrogen pointing towards the active site. This flexibility of Gln50 is in line with previous studies that showed a small contribution of the oxyanion hole with respect to the solution reaction.[18,19] One key observation is that the cis conformation of Gly83 and Cys84 is stabilized thanks to the presence of a water molecule that is hydrogen bonded to both carbonyl backbones of Gly83 and Pro45, and additionally to the nitrogen of the indole ring of Trp44. This water molecule together with the amide of Cys84, and in some conformations the sidechain of Gln50, correspond to the oxyanion hole of HG3.17. Interestingly, the positioning of the nitrogen indole of Trp44 outside the catalytic pocket reduces Gln50 flexibility thus enhancing Gln50 preorgani-

zation. In this other Trp44 rotamer, Gln50 establishes hydrogen bonds with the Pro45 backbone via an ordered water molecule and with the indole nitrogen of the other Trp87 residue, helping to maintain Gln50 close to 6NT/5NT. This interplay between Gln50 and Trp44 positioning induced by distal active site mutations affects the network of hydrogen bonding, Gln50 preorganization, and water content of the active site pocket. The additional flexibility of Gln50 regulated by Trp44 conformation observed in HG3.17 can potentially help substrate binding and product release. Our study therefore shows how active site, but especially distal mutations introduced along the evolutionary pathway enhance the conformational flexibility of the starting enzyme scaffold, which is crucial for oxyanion hole preorganization, fine-tuning the water-mediated network of non-covalent interactions and promoting substrate binding/product release. These results have implications in enzyme design, as it evidences the importance of the conformational flexibility of the starting enzyme scaffold, and how the evaluation of conformational landscapes and complex enzymatic network of non-covalent interactions can potentially advance computational enzyme design one step further.

Acknowledgements

We thank the Generalitat de Catalunya for the consolidated group TCBioSys (SGR 2021 00487), Spanish MICIN for grant projects PID2021-129034NB–I00 and PDC2022-133950-I00. S.O. is grateful to the funding from the European Research Council (ERC) under the European Union's Horizon 2020 research and innovation program (ERC-2015-StG-679001, ERC-2022-POC-101112805, ERC-2023-POC-101158166, and ERC-2022-CoG-101088032), and the Human Frontier Science Program (HFSP) for project grant RGP0054/2020. H.D. was supported by a predoctoral grant from Spanish project PID2021-129034NB–I00 and HFSP (RGP0054/2020). J.S. was supported by the Spanish MINECO for a PhD fellowship (PRE2022-105114), and D. R. M. by a research grant from HFSP (RGP0054/2020).

Conflict of Interests

The authors declare no conflict of interest.

Data Availability Statement

The data that support the findings of this study are available from the corresponding author upon reasonable request.

Keywords: Kemp elimination · Molecular dynamics simulations · Non-covalent Interactions · Shortest path map · Enzyme design

[1] a) A. Warshel, P. K. Sharma, M. Kato, Y. Xiang, H. Liu, M. H. M. Olsson, *Chem. Rev.* **2006**, *106*, 3210–3235; b) S. Marti, M. Roca, J. Andres, V. Moliner, E. Silla, I. Tunon, J. Bertran, *Chem. Soc. Rev.* **2004**, *33*, 98–107.
[2] J. Åqvist, M. Kazemi, G. V. Isaksen, B. O. Brandsdal, *Acc. Chem. Res.* **2017**, *50*, 199–207.
[3] N. Tokuriki, D. S. Tawfik, *Science* **2009**, *324*, 203–207.
[4] a) Campbell, M. Kaltenbach, G. J. Correy, P. D. Carr, B. T. Porebski, E. K. Livingstone, L. Afriat-Jurnou, A. M. Buckle, M. Weik, F. Hollfelder, N. Tokuriki, C. J. Jackson, *Nat. Chem. Biol.* **2016**, *12*, 944–950; b) R. M. Crean, J. M. Gardner, S. C. L. Kamerlin, *J. Am. Chem. Soc.* **2020**, *142*, 11324–11342; c) M. A. Maria-Solano, E. Serrano-Hervás, A. Romero-Rivera, J. Iglesias-Fernández, S. Osuna, *Chem. Commun.* **2018**, *54*, 6622–6634; d) D. Petrović, V. A. Risso, S. C. L. Kamerlin, J. M. Sanchez-Ruiz, *J. R. Soc. Interface* **2018**, *15*, 20180330.
[5] S. Osuna, *WIREs Computat. Mol. Sci.* **2021**, *11*, e1502
[6] G. Kiss, N. Çelebi-Ölçüm, R. Moretti, D. Baker, K. N. Houk, *Angew. Chem. Int. Ed.* **2013**, *52*, 5700–5725.
[7] Y. Miao, R. Metzner, Y. Asano, *ChemBioChem* **2017**, *18*, 451–454.
[8] D. Röthlisberger, O. Khersonsky, A. M. Wollacott, L. Jiang, J. DeChancie, J. Betker, J. L. Gallaher, E. A. Althoff, A. Zanghellini, O. Dym, S. Albeck, K. N. Houk, D. S. Tawfik, D. Baker, *Nature* **2008**, *453*, 190–195.
[9] F. Richter, A. Leaver-Fay, S. D. Khare, S. Bjelic, D. Baker, *PLoS ONE* **2011**, *6*, e19230.
[10] a) I. V. Korendovych, D. W. Kulp, Y. Wu, H. Cheng, H. Roder, W. F. DeGrado, *Proc. Natl. Acad. Sci. USA* **2011**, *108*, 6823–6827; b) M. Merski, B. K. Shoichet, *Proc. Natl. Acad. Sci. USA* **2012**, *109*, 16179–16183; c) V. A. Risso, S. Martinez-Rodriguez, A. M. Candel, D. M. Krüger, D. Pantoja-Uceda, M. Ortega-Muñoz, F. Santoyo-Gonzalez, E. A. Gaucher, S. C. L. Kamerlin, M. Bruix, J. A. Gavira, J. M. Sanchez-Ruiz, *Nat. Commun.* **2017**, *8*, 16113.
[11] a) O. Khersonsky, G. Kiss, D. Roethlisberger, O. Dym, S. Albeck, K. N. Houk, D. Baker, D. S. Tawfik, *Proc. Natl. Acad. Sci. USA* **2012**, *109*, 10358–10363; b) O. Khersonsky, D. Röthlisberger, O. Dym, S. Albeck, C. J. Jackson, D. Baker, D. S. Tawfik, *J. Mol. Biol.* **2010**, *396*, 1025–1042; c) O. Khersonsky, D. Röthlisberger, A. M. Wollacott, P. Murphy, O. Dym, S. Albeck, G. Kiss, K. N. Houk, D. Baker, D. S. Tawfik, *J. Mol. Biol.* **2011**, *407*, 391–412; d) H. K. Privett, G. Kiss, T. M. Lee, R. Blomberg, R. A. Chica, L. M. Thomas, D. Hilvert, K. N. Houk, S. L. Mayo, *Proc. Natl. Acad. Sci. USA* **2012**, *109*, 3790–3795; e) R. Blomberg, H. Kries, D. M. Pinkas, P. R. Mittl, M. G. Grutter, H. K. Privett, S. L. Mayo, D. Hilvert, *Nature* **2013**, *503*, 418–421.
[12] A. Broom, R. V. Rakotoharisoa, M. C. Thompson, N. Zarifi, E. Nguyen, N. Mukhametzhanov, L. Liu, J. S. Fraser, R. A. Chica, *Nat. Commun.* **2020**, *11*, 4808.
[13] R. Otten, R. A. P. Pádua, H. A. Bunzel, V. Nguyen, W. Pitsawong, M. Patterson, S. Sui, S. L. Perry, A. E. Cohen, D. Hilvert, D. Kern, *Science* **2020**, *370*, 1442–1446.
[14] K. Świderek, I. Tuñón, V. Moliner, J. Bertran, *ACS Catal.* **2015**, *5*, 2587–2595.
[15] J. Na, K. N. Houk, D. Hilvert, *J. Am. Chem. Soc.* **1996**, *118*, 6462–6471.
[16] H. Kries, J. S. Bloch, H. A. Bunzel, D. M. Pinkas, D. Hilvert, *ACS Catal.* **2020**, *10*, 4460–4464.
[17] a) P. Bryan, M. W. Pantoliano, S. G. Quill, H. Y. Hsiao, T. Poulos, *Proc. Natl. Acad. Sci. USA* **1986**, *83*, 3743–3745; b) J. D. Robertus, J. Kraut, R. A. Alden, J. J. Birktoft, *Biochemistry* **1972**, *11*, 4293–4303; c) W. W. Bachovchin, *Magn. Reson. Chem.* **2001**, *39*, S199–S213.
[18] J. P. Schwans, F. Sunden, A. Gonzalez, Y. Tsai, D. Herschlag, *J. Am. Chem. Soc.* **2011**, *133*, 20052–20055.
[19] D. A. Kraut, P. A. Sigala, T. D. Fenn, D. Herschlag, *Proc. Natl. Acad. Sci. USA* **2010**, *107*, 1960–1965.
[20] P. Wang, J. Zhang, S. Zhang, D. Lu, Y. Zhu, *J. Chem. Inf. Model.* **2023**, *63*, 1323–1337.
[21] H. A. Bunzel, H. Kries, L. Marchetti, C. Zeymer, P. R. E. Mittl, A. J. Mulholland, D. Hilvert, *J. Am. Chem. Soc.* **2019**, *141*, 11745–11748.
[22] F. Peccati, E. L. Noey, K. N. Houk, S. Osuna, G. Jiménez-Osés, *ChemCatChem* **2024**, *16*, e202400444.
[23] J. Contreras-García, E. R. Johnson, S. Keinan, R. Chaudret, J.-P. Piquemal, D. N. Beratan, W. Yang, *J. Chem. Theory Comput.* **2011**, *7*, 625–632.
[24] S. Ramsey, C. Nguyen, R. Salomon-Ferrer, R. C. Walker, M. K. Gilson, T. Kurtzman, *J. Comput. Chem.* **2016**, *37*, 2029–2037.

Manuscript received: October 9, 2024
Accepted manuscript online: November 14, 2024
Version of record online: November 28, 2024